



1 **Exploring the inconsistent variations in atmospheric primary and**
2 **secondary pollutants during the G20 2016 Summit in Hangzhou, China:**
3 **implications from observation and model**

4 **Gen Zhang^{1*}, Honghui Xu^{2*}, Hongli Wang³, Likun Xue⁴, Jianjun He¹, Wanyun Xu¹, Bing Qi⁵,**
5 **Rongguang Du⁵, Chang Liu¹, Zeyuan Li⁴, Ke Gui¹, Wanting Jiang⁶, Linlin Liang¹, Yan Yan¹,**
6 **Xiaoyan Meng⁷**

7 ¹ State Key Laboratory of Severe Weather & Key Laboratory of Atmospheric Chemistry of CMA,
8 Chinese Academy of Meteorological Sciences, Beijing 100081, China

9 ² Zhejiang Institute of Meteorological Science, Hangzhou 310008, China

10 ³ State Environmental Protection Key Laboratory of Formation and Prevention of Urban Air Pollution
11 Complex, Shanghai Academy of Environmental Sciences, Shanghai 200233, China

12 ⁴ Environment Research Institute, Shandong University, Ji'nan, Shandong 250100, China

13 ⁵ Hangzhou Meteorological Bureau, Hangzhou 310051, China

14 ⁶ Plateau Atmospheric and Environment Laboratory of Sichuan Province, College of Atmospheric
15 Science, Chengdu University of Information Technology, Chengdu 610225, China

16 ⁷ State Environmental Protection Key Laboratory of Quality Control in Environmental Monitoring,
17 China National Environmental Monitoring Centre, Beijing 100012, China

18 *Correspondence to:* Gen Zhang (zhanggen@cma.gov.cn) and Honghui Xu (forsnow@126.com)

19 **Abstract.** Complex aerosol and photochemical pollution (ozone and peroxyacetyl nitrate (PAN))
20 frequently occur in eastern China and mitigation strategies to effectively alleviate both kinds of pollution
21 are urgently needed. Although the effectiveness of powerful control measures implemented by the
22 Chinese State Council has been comprehensively evaluated on reducing atmospheric primary pollutants,
23 the effectiveness on mitigating photochemical pollution is less assessed and therein the underlying
24 mechanisms are still poorly understood. The stringent emission controls implemented from 24 August to
25 6 September, 2016 during the summit for Group of Twenty Finance Ministers and Central Bank
26 Governors (G20) provides us a unique opportunity to address this issue. Surface concentrations of
27 atmospheric O₃, PAN, and their precursors including volatile organic compounds (VOCs) and nitrogen
28 dioxides (NO_x), in addition to the other trace gases and particulate matter were measured at the National
29 Reference Climatological Station (NRCS) (30.22 °N, 120.17 °E, 41.7 m a.s.l) in urban Hangzhou. We
30 found significant decreases in atmospheric PAN, NO_x, the total VOCs, PM_{2.5}, and sulfur dioxide (SO₂)
31 under the unfavorable meteorological condition during G20 (DG20) relative to the adjacent period
32 before and after G20 (BG20 and AG20), indicating that the powerful control measures have taken into
33 effect on reducing the pollutants emissions in Hangzhou. Unlike with the other pollutants, daily
34 maximum average-8 h (DMA8) O₃ exhibited a slight increase and then decrease from BG20 to AG20,



35 which was mainly attributed to the variation in the solar irradiation intensity and regional transport
36 besides the contribution from the implement of stringent control measures. Results from
37 observation-based chemical model (OBM) indicated that acetaldehyde and methyl glyoxal (MGLY)
38 were the most important second-generation precursors of PAN, accounting for 37.3-51.6% and
39 22.8%-29.5% of the total production rates including the reactions of OVOCs, propagation of other
40 radicals, and the other minor sources. Moreover, we confirmed the productions of PAN and O₃ were both
41 sensitive to VOCs throughout the whole period, specifically dominated by aromatics in BG20 and DG20
42 but alkenes in AG20. These findings suggested that reducing emissions of aromatics, alkenes, and alkanes
43 would mitigate photochemical pollution including PAN and O₃. Source appointment results attribute the
44 reductions of VOCs source and ozone formation potentials (OFP) during G20 to the effective emission
45 controls on traffic (vehicle exhaust) and industrial processes (solvent utilization and industrial
46 manufacturing). However, fuel combustion and biogenic emission both weakened such effect with
47 sizeable contribution on the VOCs mixing ratios (18.8% and 20.9%) and OFPs (25.6% and 17.8%),
48 especially during the latter part of G20 (G20 II) when anthropogenic VOCs were substantially reduced.
49 This study highlights the effectiveness of stringent emission controls in relation to traffic and industrial
50 sources, but a coordinated program related with controlling fuel combustion and biogenic emissions is
51 also required on addressing secondary pollution.

52 **1 Introduction**

53 Complex atmospheric pollution including particulate and photochemical pollution (ozone (O₃) and
54 peroxyacetyl nitrate (PAN)) is a pervasive environmental issue in eastern China (Geng et al., 2007;
55 Ding et al., 2013; Mo et al., 2015; Li et al., 2016; Zhang et al., 2018). Numerous mitigation strategies
56 have been released by the Chinese government, such as the nationwide application of flue-gas
57 desulfurization (FGD) devices in power plants after 2006 (Feng et al., 2014) and “Atmospheric
58 Pollution Prevention and Control Action Plan” in 2013 (Zhang et al., 2016). As expected, ambient
59 concentrations of primary gas pollutants such as sulfur dioxide (SO₂) (Koukouli et al., 2016) and
60 nitrogen oxides (NO_x = NO + NO₂) (de Foy et al., 2016) showed good response to emission reductions.
61 However, secondary atmospheric pollutants such as ozone and secondary aerosols, which are dominant
62 compounds of fine particulate matter, frequently exceeded their respective Chinese Grade II standards
63 over urban cities in China (Wang et al., 2014). Severe haze pollution, mainly comprised of PM_{2.5}
64 (particles within 2.5 μm diameter range), still occur in China during wintertime, although it started to
65 decline during the 11th Five-Year Plan period (Huang et al., 2014; Cheng et al., 2016; Miao et al., 2018;
66 Miao and Liu, 2019). Surface O₃ also exhibits a rapid increasing trend over China since 2000
67 (Verstraeten et al., 2015; Wang et al., 2017), with high levels (9.5-14.0 ppbv) of PAN often encountered
68 during O₃ pollution events (Shao et al., 2009; Liu et al., 2010; Zhang et al., 2012a; Zhang et al., 2014;
69 Zhang et al., 2015; Xue et al., 2014c). Due to the highly nonlinear response of O₃ and PAN to primary



70 pollutant emissions, the mitigation of secondary photochemical pollution is even more challenging. In
71 the troposphere, O₃ and PAN are both formed in photochemical reactions of VOCs in the presence of
72 NO_x. However, PAN is exclusively formed by the oxidation of a small part of VOCs that can generate
73 peroxy acetyl radical (CH₃C(O)O₂, PA) including oxygenated VOCs (OVOCs) such as acetaldehyde,
74 acetone, methacrolein (MACR), methyl vinyl ketone (MVK), and methyl glyoxal (MGLY) (Williams et
75 al., 2000; LaFranchi et al., 2009), while O₃ formation involves almost all VOCs. Therefore, PAN is
76 considered to be a better indicator for photochemical smog than O₃ (McFadyen and Cape, 2005). In
77 addition, these OVOCs are mainly oxidation products (here referred to secondary precursors of PAN) of
78 a certain class of hydrocarbons (e.g., ethane, propene, isoprene, and some aromatics) by the oxidations
79 of OH/NO₃/O₃. The relative importance of individual precursors to the formation of PAN and O₃ varies
80 from place to place depending on the reactivity and composition of VOCs. Identification of the
81 dominant precursors is the key to effective control of photochemical pollution, which, however, remains
82 poorly characterized in China.

83 Recently, a series of temporary and stringent emission control measures were implemented in China
84 during several mega-events including the 29th Summer Olympic Games (August 2008), the 21th
85 Asia-Pacific Economic Cooperation (APEC) conference (November 2014), and China Victory Day
86 Parade (Victory Parade 2015) in Beijing (Verstraeten et al., 2015) and the surrounding areas (Xu et al.,
87 2010; Zhang et al., 2012b; Gao et al., 2011; Li et al., 2017). During these events, the effectiveness of a
88 series of emission control measures on reducing atmospheric primary pollutants, in particular to the
89 particulate matter, has been comprehensively evaluated, but the effectiveness on photochemical
90 pollution are less evaluated.

91 In September 2016, the Group of Twenty (G20) summit was hosted in Hangzhou, the capital city of
92 Zhejiang Province, which is located along the mid-Yangtze River Delta (YRD) in the eastern part of
93 China. Similar with other major events held in Beijing, rigorous temporal control measures were set to
94 reduce emissions of air pollutants in Hangzhou and the adjacent regions including Zhejiang, Shanghai,
95 Jiangsu, and Anhui province from 24 August to 7 September. These control measures included
96 restrictions on the number of vehicles, limited production or complete shut-down of industrial
97 enterprises, and temporary cessation of construction activities, and the target sources incorporated
98 vehicles, paint and solvent use, steel factories, chemical factories, power plants. In this study, to
99 evaluate the effectiveness of emission control measures on reducing pollutant concentrations, we
100 compared the variations of atmospheric O₃, PAN, particulate matter, VOCs, NO_x, and other trace gases
101 before, during, and after G20, also demonstrating the effect of meteorological conditions by using
102 WRF-Chem model. An observation-based chemical box model (OBM) was used to identify the
103 predominant precursors and key chemical processes in PAN and O₃ formation and to further assess the
104 effect of reducing their respective precursors before, during, and after G20. Positive matrix factorization
105 (PMF) was employed to appoint the corresponding sources of various VOCs and compare their



106 variations and their respective ozone formation potentials (OFPs) before, during, and after G20.

107 **2. Experimental**

108 **2.1 Observations**

109 In-situ observations of atmospheric PAN, O₃, and VOCs and a suite of associated chemical species and
110 meteorological parameters, including NO_x, CO, SO₂, fine particulate matter (PM_{2.5}), were conducted at
111 an urban site named as National Reference Climatological Station (NRCS) (30.22°N, 120.17°E, 41.7 m
112 a.s.l) in the center of Hangzhou as shown in Figure S1 in Supplement (SI). PAN was measured by a
113 modified gas chromatography (Agilent 7890B, USA) equipped with electron capture detector, which
114 has been described in our previous studies in details (Zhang et al., 2012a; Zhang et al., 2014; Zhang et
115 al., 2015). Trace gases including O₃, SO₂, NO_x, and CO were detected by a set of commercial trace gas
116 analyzers (Thermo Environmental Instruments Inc., USA i-series 49i, 43i, 42i, and 48i), respectively
117 (Zhang et al., 2018). Ambient VOCs were measured by using an on-line gas chromatography (Syntech
118 Spectras Instrument Co., Ltd., The Netherlands) coupled with dual detectors (Photo Ionization Detector
119 (PID) and flame ionization detector (FID) for quantifying C₂-C₅ VOCs (GC955 series 811) and PID for
120 detecting C₆-C₁₂ VOCs (GC955 series 611). Ambient PM_{2.5} samples were collected using co-located
121 Thermo Scientific (formerly R&P) Model 1405D samplers.

122 **2.2 Models**

123 **2.2.1 WRF-Chem model**

124 To quantify the separate effects of meteorological condition (EMC) and emission control measures
125 (EEC) on observed particulate concentrations, we performed simulations using Weather Research and
126 Forecasting model coupled to Chemistry (WRF-Chem). WRF-Chem V3.9 was used to simulate the
127 variation of PM_{2.5} concentration from Aug. 6 00:00 UTC, 2016 to Sep. 16 00:00 UTC, 2016.
128 Multi-resolution Emission Inventory for China at 0.25° in 2016, developed by Tsinghua University
129 (<http://www.meicmodel.org/>), was used as input for WRF-Chem. WRF-Chem was configured to have
130 two nested domains, i.e. an outer domain with horizontal resolution of 25 km (140×100 grid points)
131 covering East China and the surrounding areas and an inner domain with 5 km-resolution (101×101 grid
132 points) covering Yangtze River Delta. Hangzhou is located in the center of domain. Vertically, there
133 were a total of 35 full eta levels extending to the model top at 50 hPa, with 16 levels below 2 km. The
134 National Centers for Environmental Prediction (NCEP) Final Operational Global Analysis (FNL) data
135 available at 1°×1° every six hours were used meteorological driving fields. Analysis nudging was used
136 for domain one. RADM2 chemical mechanism and MADE/SORGAM aerosols were used in this study.
137 In principle, the net contribution (NCC) of emission controls and meteorological conditions primarily
138 results in the difference between observed PM_{2.5} before and during G20, which is represented by the
139 ratio of (Observed PM_{2.5} (BG20)- Observed PM_{2.5} (DG20 II))/Observed PM_{2.5} (BG20). The effect of



140 meteorological conditions (EMC) was quantified by comparing the modeled $PM_{2.5}$ without emission
141 controls before and during G20 under their respective meteorological condition (Equation 1). Thereby,
142 the effect of emission controls (ECC) could be obtained through the difference between NCC and EMC
143 before and during G20 (Equation 2) below

$$EMC = \frac{Modeled\ PM_{2.5}(BG20) - Modeled\ PM_{2.5}(DG20\ II)}{Modeled\ PM_{2.5}(BG20)} \times 100\% \quad (1)$$

$$ECC = (NCC - EMC) \times 100\% \quad (2)$$

144 In general, the modeled results of $PM_{2.5}$ before and after G20 can reproduce the observation results
145 (mean bias (MB) = 2.46, root mean-square error (RMSE) = 15.5, $R = 0.63$, $p < 0.01$), providing the basis
146 of the following comparison.

147 2.2.2 Backward trajectories analysis

148 To determine the influence of regional transport on the pollutant concentrations, 24 h air mass back
149 trajectories starting at 300 m from NRCS site were calculated by using the National Oceanic and
150 Atmospheric Administration (NOAA) HYSPLIT-4 model with a $1^\circ \times 1^\circ$ grid and the final meteorological
151 database. The 6-hourly final archive data were obtained from the National Center for Environmental
152 Prediction's Global Data Assimilation System (GDAS) wind field reanalysis. GDAS uses a spectral
153 medium-range forecast model. More details can be found at <http://www.arl.noaa.gov/ready/open/hysplit4.html>. The model was run 24 times per day. The method used in trajectory
154 clustering was based on the GIS-based software TrajStat (Wang et al., 2004).
155

156 2.2.3 Observation-based chemical box model (OBM)

157 Here we used OBM model to simulate in situ PAN and O_3 production and their sensitivity to changes in
158 PAN and O_3 precursors, which has been successfully implied in our previous studies (Xue et al., 2014a;
159 Xue et al., 2014c; Xue et al., 2016; Li et al., 2018). In brief, the model was built on the latest version of
160 the Master Chemical Mechanism (MCM v3.3), an explicit mechanism describing the degradation of 143
161 primarily emitted VOC, resulting in 17,224 reactions involving 5833 molecular and free radical species
162 (Saunders et al., 2003). Besides the existing reactions in MCM v3.3, the heterogeneous reactions of
163 NO_2 , HO_2 , NO_3 , and N_2O_5 were also incorporated. In addition, we also optimized the model with some
164 physical processes such as the variations of boundary layer height and solar zenith angle, dry deposition,
165 and the dilution of air pollutants within the planetary boundary layer (Xue et al., 2014b). The photolysis
166 frequencies appropriate for Hangzhou are parameterized using a two-stream isotropic-scattering model
167 under clear sky conditions. In this study, all of these reactions were tracked and grouped into a small
168 number of formation pathways, such as acetaldehyde, acetone, MACR, MVK, MGLY, other OVOCs,
169 reactions of O_3 with isoprene and MPAN, and propagation of other radicals to PA. The production rate
170 of PA could be estimated as the sum of these reaction rates. The ozone production rates were calculated



171 through the oxidation of NO by HO₂ and RO₂, and its destruction rates were mainly facilitated by O₃
172 photolysis and reaction with NO, NO₂, OH, HO₂, and unsaturated VOCs. Moreover, we investigated the
173 sensitivities of PAN and O₃ formation to their respective precursor species by introducing a relative
174 incremental reactivity (RIR) concept which is widely applied in the OBM investigation of PAN and
175 ozone formation (Chameides et al., 1999; Xue et al., 2014c). In this calculation, we performed model
176 calculations during the period of 20 August-10 September, 2016, during which the VOCs measurement
177 were available. The model was run based on the hourly average profiles of PAN, O₃, CO, SO₂, NO, NO₂,
178 C₂-C₁₀ NMHCs, air temperature and pressure, and RH measured at NRCS site. During the simulation,
179 the model was pre-run for three days with constrain of the data of 20-22 August so that it reached a
180 steady state for the unmeasured species (e.g., MACR, MVK, HONO, radicals). More detailed
181 description of this model has been given in previous studies (Jenkin et al., 2003; Xue et al., 2014a; Xue
182 et al., 2014c).

183 2.2.4 Positive matrix factorization (PMF) Model

184 Positive matrix factorization (PMF) is an effective source apportionment receptor model based on the
185 fingerprints of the sources that does not require the source profiles prior to analysis and has no
186 limitation on source numbers (Hopke, 2003; Pentti and Unto, 1994). The data used in PMF is of the
187 form of an $i \times j$ matrix X , in which i is the sampling number and j is the number of species. Based on
188 chemical mass balance of the pollutants, the following equation can be derived as:

$$X_{ij} = \sum_{k=1}^p g_{ik} f_{ik} + e_{ij}$$

189 where p is the number of the sources (i.e., the number of factors), f is the profile of each source, g refers
190 to the contribution of each factor to the total concentration, and e is the residual. Factor contributions
191 and profiles are derived by minimizing the total scaled residual Q :

$$Q = \sum_{i=1}^n \sum_{j=1}^m \left(\frac{e_{ij}}{u_{ij}} \right)^2$$

192 where u is the uncertainty of the sampling data. More details about principles have been found
193 elsewhere (Cai et al., 2010; Zhang et al., 2013; Li et al., 2017; Li et al., 2015). In this study, we used
194 EPA PMF 5.0 model to identify major VOCs sources and their temporal variations. We discarded the
195 species that were below MDL for more than 50% of the time or showed a significantly smaller signal to
196 noise ratio (S/N). The uncertainties for each sample and species were calculated based on the following
197 equation if the concentration is greater than the method detection limit (MDL) provided:

$$\text{Uncertainty} = \sqrt{(0.5 \times \text{DML})^2 + (\text{Error Fraction} \times \text{Concentration})^2}$$

198 Values below the detection limit were replaced by one-half of the MDL and their overall uncertainties
199 were set at five-sixths of the MDL values. In this analysis, different numbers of factors were tested. The
200 robust mode was used to reduce the influence of extreme values on the PMF solution. More than 95% of



201 the residuals were between -3 and 3 for all compounds. The Q values in the robust mode were
202 approximately equal to the degrees of freedom.

203 **3 Results and discussion**

204 In order to comprehensively evaluate air quality during the G20 period, we compared the concentrations
205 of pollutants during G20 with the adjacent time period in 2016, respectively. According to the control
206 measures schemes, we classified the whole period into three episodes: one week before G20 (BG20)
207 (16-23 August, 2016), during G20 (DG20) (24 August-6 September) including Phase I (24-27 August)
208 and Phase II (28 August-6 September), and one week after G20 (AG20) (7-15 September). During
209 phase I the government implemented strict emission control measures in industrial source, power plant,
210 and residential and the phase II referred to the additional controls measures as vehicles controls in the
211 Hangzhou and surrounding provinces (including Zhejiang, Jiangsu, Jiangxi, and Anhui).

212 **3.1 Evolutions of meteorological condition**

213 First, we looked into the day-to-day variations of meteorological parameters and atmospheric pollutants
214 from BG20 to AG20 in Fig. S2 in SI. In the period of BG20 and the beginning of DG20 I (16-25
215 August), subtropical anticyclone dominated the Hangzhou and surrounding area, leading to continuous
216 10 days with daily mean temperature of 31.5 °C ranged from 29.9-32.5 °C and strong solar irradiation
217 intensity (mean daily maximum value: 369.4 W m⁻²), favorable for the photochemical production of O₃
218 and PAN. The highest O₃ (113.4 ppbv) occurred at 13:00 LT on 25 August under the maximum air
219 temperature of 35.2 °C. Meanwhile, the mean daily maximum height of mixing boundary layer (MBL)
220 during this period was up to ca. 1895 m, beneficial for the diffusion of atmospheric primary pollutants
221 in the vertical direction. In addition, the prevailing wind was from east (15.1%) with a mean wind speed
222 of 2.9 m s⁻¹. Results from the backward trajectory simulations demonstrated that the air masses from the
223 east originated from the East China Sea and Yellow Sea, bringing in clean marine air (Fig. S3). Thus,
224 meteorological conditions before G20 were favorable for the dispersal of atmospheric pollutants. On 26
225 and 27 August, the weather pattern changed to a cold continental high with showery and windy days.
226 The total precipitation and mean wind speed both reached their respective maximums of 14.6 mm and
227 3.7 m s⁻¹ on 26 August. Accordingly, all species except CO significantly decreased by 12.3% for SO₂,
228 29.7% for NO_x, 6.7% for PM_{2.5}, 11.9% for daily maximum average-8 h (DMA8) O₃, and 56.1% for
229 PAN relative to BG20. With respect to the last half of DG20 I and the beginning of DG20 II (28-31
230 August), the prevailing wind experienced a shift from northwest to west and to southwest. On 28
231 August, the prevailed wind was from the north with the average daily maximum wind speed of 3.9 m s⁻¹
232 during G20, and the relative humidity rapidly decreased by 26.2% relative to the previous day. As seen
233 in Fig. S3, air masses arrived at Hangzhou from the north passed through all of Jiangsu Province and
234 northern parts of Zhejiang Province, two of the most developed provinces in China, with intense human



235 activities. They carried higher $PM_{2.5}$, SO_2 , NO_x , and CO loadings than the other clusters (See Table S1).
236 On 1 September, the prevailing wind was from southwest with high wind speeds (3.3 m s^{-1}). Results
237 from back trajectories indicated that the southwesterly air masses originated from northern Jiangxi
238 Province, transported over western Zhejiang Province, and arrived at Hangzhou, with high
239 concentration loadings of SO_2 , particulate matter, O_3 , and PAN. The increased relative humidity (56.5%)
240 relative to 49.5% on 31 August was beneficial for the formation of particulate matter. During 2-4
241 September, Hangzhou area witnessed a stable meteorological condition with weak wind ($WS < 2.6 \text{ m/s}$),
242 continuously high air temperature (daily maximum average: $32.2 \text{ }^\circ\text{C}$), and moderate relative humidity
243 (ca. 60%). Such condition was favorable for the accumulation of particulate matter and the
244 photochemical production of O_3 . It caused significant increases by 25.1% for $PM_{2.5}$, 16.7% for PM_{10} ,
245 and 10.7% for O_3 compared with BG20, in contrast to the large decreases by 56.4% for SO_2 and 27.9%
246 for NO_x due to the implement of emission control measures. Overall, the meteorological condition
247 during G20 II was not favorable for the dispersal of atmospheric primary pollutants but beneficial for
248 producing O_3 . However, with the proceeding of the stringent control measures, the most distinct drops
249 of pollutants concentrations were found on 5 September, with the large reductions of 50.0% for $PM_{2.5}$,
250 18.3% for DMA8 O_3 , 55.7% for SO_2 , 41.3% for NO_x , and 65.6% for PAN relative to BG20, respectively.
251 Within AG20, 7 rainy days with mean daily total precipitation of 18.7 mm occurred as well as 6 days
252 with low wind speed (ca. 2.0 m/s) and 8 days with low MBL ($<1000 \text{ m}$). Such meteorological condition
253 was beneficial for scavenging the particulate matter and SO_2 by wet deposition in addition to the
254 accumulation of NO_x . In addition, weak solar irradiation intensity was not favorable for the
255 photochemical formation of O_3 and PAN. On 7 September a moderate showery lasted from 2:00 LT to
256 11:00 LT with daily total precipitation of 9.5 mm, accompanied by low air temperature ($21.5 \text{ }^\circ\text{C}$) and
257 wind speed (1.8 m/s). Compared with the previous day, significant decreases of DMA8 O_3 (22.6%) was
258 found as expected, while together with a small reduction ratio of $PM_{2.5}$ (2.7%) and unexpected increases
259 for NO_x (41.1%) and SO_2 (175.1%), indicating that emissions immediately bounced back after lifting
260 the ban on emission controls.

261 3.2 Evolutions of pollutant concentrations

262 Statistically, observed daytime concentrations of $PM_{2.5}$, NO_x , and SO_2 in DG20 II both exhibited
263 significant decreases relative to those in BG20 with the reduction ratios of 11.3%, 17.0%, and 18.0%,
264 respectively (Fig. 1). Furthermore, by using WRF-Chem model we quantified the contributions of the
265 emission control measures (ECC) with 63.5%, 44.1%, and 31.2% to the reductions of $PM_{2.5}$, SO_2 , and
266 NO_2 in DG20 II relative to BG20, respectively, but for the meteorological conditions it made negative
267 contributions. This evidence well indicated that powerful control measures have taken into effect on
268 reducing pollutant emissions in Hangzhou under the unfavorable meteorological conditions. The large
269 decreases of NO_x and SO_2 reflected the reduction of vehicle exhaust and coal consumption during G20



270 in Hangzhou and surrounding areas. It is worth noting that CO showed gradual increases (ca. 20.7%)
271 from BG20 to DG20. Fuel combustions, mainly including residential usage and liquid natural gas and
272 petroleum gas, around YRD regions during this period might account for such unique pattern of CO.
273 Under the same stringent control measures, the variation of O₃ was not consistent with the primary
274 pollutants. Observed DMA8 O₃ increased by 12.4% in DG20 I relative to BG20, which was attributed
275 to regional transport from the northern provinces and the enhanced solar radiation intensity. Afterwards,
276 DMA8 O₃ decreased by 33.4% from DG20 II to AG20 (Fig. 1), as did the peak values of mean daily O₃
277 in DG20 II compared to BG20 and DG20 I (Fig. S4). This evidence suggests that additional vehicles
278 controls implemented during DG20 II might have played an important role in reducing atmospheric O₃
279 pollution in Hangzhou reflected by shaping such unique diurnal variation, which was also confirmed by
280 the decreased OFP from vehicle exhaust below. Elevated O₃ during DG20 rush hours (as shown in Fig.
281 S2 and S3) was attributed to the reduced titration of fresh NO emission under the control measures on
282 vehicle exhaust. Considering such effects, O_x (represented by the sum of O₃+NO₂) was used to
283 determine the local photochemical formation. The variation of DMA8 O_x was similar with O₃, with
284 distinct decreasing trend from DG20 II to AG20. For PAN, it showed different pattern with O₃. Daytime
285 PAN exhibited significant decrease (ca. 45.4%) found from BG20 to DG20 II and then it sharply built
286 up to similar magnitudes in AG20 with BG20. Thereby, it both indicates the significant effectiveness of
287 emission control measures on reducing local photochemical formation of O₃ and PAN. The underlying
288 formation mechanisms of PAN and O₃ including their respective key precursors and chemical process
289 are elucidated in Sect.3.3.

290 With respect to VOCs, the mixing ratios of total VOCs also showed significant reduction of 20.0% in
291 DG20 compared with BG20, but increased by 104.1% in AG20 after control (Table S2). Alkanes were
292 the most abundant VOCs group (55.4%) in all periods, and were reduced by 19.8% from BG20 to DG20.
293 On the contrary, alkenes increased by 20.0% in DG20 compared to BG20, among which ethylene
294 accounted for 63.9%-78.0% during the three periods, although other alkenes decreased to a minor extent.
295 As expected, aromatics were reduced by 49.7% in DG20 compared with BG20. Ambient mixing ratios
296 of specific VOCs at NRCS station are summarized in Table S3. Ethane, ethylene, benzene, and toluene
297 are the four most abundant species during all the periods. Compared with BG20, except ethane,
298 isopentane, and ethylene, the mixing ratios of all species decreased in DG20. Ethylene, as a
299 representative tracer of fuel combustion, showed continuous increase from BG20 to AG20, possibly
300 indicating the ineffectiveness of control measures in this source.

301 **3.3 Identification of the Key Precursors and Chemical Processes for PAN and O₃**

302 To identify the key precursors and chemical processes for PAN, we employed the observation-based
303 model to investigate the daytime average contributions to PA radical production rates directly from
304 individual pathways for these four episodes (Fig. 2). Acetaldehyde (e.g., oxidation of OH and NO₃) and



305 MGLY (e.g., photolysis and oxidation by OH and NO₃) were the most important sources of PA in
306 Hangzhou, accounting for 37.3-51.6% and 22.8%-29.5% of the total production rates. This was in
307 agreement with the findings obtained from the other typical urban areas such as Beijing (Xue et al.,
308 2014c; Liu et al., 2010; Zhang et al., 2015), Tokyo (Kondo et al., 2008), Houston, Nashville (Roberts et
309 al., 2001), and Sacramento (LaFranchi et al., 2009). Reactions of OVOCs and propagation of other
310 radicals to PA (mainly including decomposition of some RO radicals and reactions of some higher acyl
311 peroxy radicals with NO) were also significant sources, with average contributions of 7.1%-9.1% and
312 18.1%-27.0%, respectively. A minor contribution (~1% in total) was originated from the other pathways
313 of O₃+isoprene, O₃+MPAN, acetone, and MVK. Acetaldehyde and other OVOCs are mainly
314 photooxidation products of hydrocarbons, thus it's necessary to further identify the first-generation
315 precursors of PAN here. We tested the model sensitivity by introducing the concept of relative
316 incremental reactivity (RIR), which is widely used in the OBM study of ozone formation (Chameides et
317 al., 1999). Here RIR is defined as the ratio of decrease in PAN production rates to decrease in precursor
318 concentrations (e.g., 20% reduction is used in this study). A number of sensitivity model runs were
319 performed to calculate the RIRs for NO_x, alkanes, alkenes, and aromatics classes as well as the
320 individual C₂-C₁₀ hydrocarbon species. As shown in Fig. 3a, production of PAN was sensitive to VOCs
321 from BG20 to AG20. Meanwhile, the negative RIR values for NO_x also indicated a VOCs regime of
322 PAN production around the G20 period in urban Hangzhou. In terms of BVOCs, the positive RIRs
323 values for isoprene (0.18-0.38) from BG20 to AG20 implied that in-situ formation of PAN at NRCS was
324 highly sensitive to isoprene. As to AVOCs, alkenes and aromatics were the most important
325 first-generation PAN precursors, with the RIRs range of 0.24-0.37 and 0.26-0.52, respectively.
326 Furthermore, we identified the other specific VOCs controlling PAN production, which were xylenes,
327 trans/cis-2-butenes, trimethylbenzenes, toluene, and propene evidenced by their positive RIRs.
328 Compared with their individual RIRs between control and non-control period, the in-situ production of
329 PAN was dominated by aromatics in BG20 and DG20 I, but controlled by alkenes in AG20. Besides
330 secondary acetaldehyde formed by the oxidation of ethanol, most aromatics were mainly emitted by
331 vehicle exhaust. The decreased RIRs of aromatics together with the decreased contribution ratios of
332 acetaldehyde to the PA radical formation during G20 both indicated the effectiveness of control
333 measures on vehicle exhaust on reducing atmospheric PAN concentration. Similar with PAN, the
334 daytime average RIRs for major groups of O₃ precursors during the episodes are shown in Fig. 3b.
335 Overall, the in-situ ozone formation was also controlled by VOCs from BG20 to AG20. AVOCs were
336 dominated by alkenes and aromatics, along with their increasing and decreasing RIRs, respectively.
337 With the proceeding of emission control, the RIR for AVOCs showed gradual decrease from BG20 to
338 DG20, but increased after G20. In contrast, BVOCs (mainly as isoprene) exhibited gradual increases for
339 all periods, especially during the phase II in DG20 and AG20 when their RIRs were both higher than
340 those for AVOCs. Thereby, the contribution of BVOCs to the photochemical production of O₃ weakened



341 the effect of stringent control measures on reducing surface O₃. The RIRs for NO_x were negative
342 throughout the period of G20, also indicating a VOC-limited regime for the sensitivity of ozone
343 formation. This suggests that reducing emissions of aromatics, alkenes, and alkanes would alleviate the
344 O₃ formation, yet cutting NO_x emissions may aggravate the local O₃ problems.

345 **3.4 Identification of VOCs sources and quantification of their respective ozone formation** 346 **potential**

347 To distinguish the various sources of VOCs, we compared the PMF profiles with the reference profiles
348 from the literature as listed below. Seven sources were identified as follows: (1) gasoline evaporation (2)
349 solvent utilization (3) industrial manufacturing (4) industrial chemical feedstock (5) vehicle exhaust (6)
350 fuel combustion (7) biogenic emission. Figure 4 exhibited the modelled source profiles together with
351 the relative contributions of each sources to individual species. The first source is characterized by a
352 significant amount (78.5%) of isopentane which is a typical tracer for gasoline evaporation (Liu et al.,
353 2008). Therefore, this source was identified as gasoline evaporation. The second source was rich in
354 n-pentane and aromatics. Many aromatics such as BTEX are the dominant components of organic paints,
355 and were regarded as chemical tracers of solvent utilization (Watson et al., 2001). Significant amounts
356 of ethylbenzene, xylenes, and n-pentane present in the second source, accounting for 19.2%, 58.8%, and
357 98.8%, respectively. Thus, the second source was identified as solvent utilization. The third source was
358 characterized by high loading of cyclohexane (54.7%) and BTEX (15.1%-46.2%). These compounds
359 are confirmed to be typical species in the industrial manufacturing in China (Liu et al., 2008). Thus, this
360 source was representative of industrial manufacturing. The fourth source identified as industrial
361 chemical feedstock (shown in Fig. 4) was characterized by a very little contribution to alkanes and
362 aromatics and large amounts of 3-ethyltoluene (29.4%), 3-methylheptane (51.0%), and n-hexane
363 (47.1%), which are typical proxies for industrial chemical feedstock (Liu et al., 2008; Mo et al., 2015).
364 The fifth source was characterized by abundant 2-methylpentane (61.7%) and BTEX, which is a typical
365 tracer for vehicle exhaust (Liu et al., 2008; Li et al., 2015). In addition, 2, 2, 4-trimethylpentane is a fuel
366 additive used to gain higher octane ratings (McCarthy et al., 2013) with high abundance of 21.4% in
367 this source and thus it is identified as vehicle exhaust. The sixth source profile shown in Fig. 4 was in
368 relation to 48.9% of the total measured ethylene mixing ratios, of which was major species emitted from
369 fuel combustion process (Li et al., 2015). It was also characterized by significant amounts of ethane,
370 propane, n-butane, propene, and benzene. Ethane and propane are the tracers of natural gas and liquid
371 petroleum gas (LPG) usage, respectively, and the source profiles of resident fuel combustion in China
372 contained alkenes (Wang et al., 2013). Coal combustion can release a large amount of BTEX into the
373 atmosphere and styrene is a typical indicator of industrial manufacturing in China (Liu et al., 2008; Li et
374 al., 2015). Thus, this source was believed to be as fuel combustion related with industrial process and
375 residual usage. The seventh source was distinguished by a significant amount of isoprene, a



376 representative indicator of biogenic emission. About 93.1% of the total isoprene mixing ratios is
377 apportioned to this factor (Guenther et al., 1995). There were very small quantities of the other species
378 such as aromatics (0-1.8%) in this factor. Therefore, it was excluded from biomass burning but mainly
379 identified as biogenic emission. Figure 5 shows the variation of the seven sources during the four
380 periods. Clearly, anthropogenic sources such as solvent utilization, industrial manufacturing, vehicle
381 exhaust, fuel combustion, and industrial chemical feedstock were the predominant sources to the total
382 VOCs before and after G20, as high as 52.4%-81.7%. Furthermore, anthropogenic emission showed
383 significant reductions during G20 response to the stringent emission control. In BG20, solvent
384 utilization was the predominant contributors to VOCs mixing ratios, contributing 1.88 ppbv, followed
385 by vehicle exhaust (1.77 ppbv, 21.6%), industrial manufacturing (1.55 ppbv, 19.0%), biogenic emission
386 (1.16 ppbv, 14.1%), gasoline evaporation (0.83 ppbv, 10.1%), and fuel combustion (0.35 ppbv, 4.3%).
387 The industry-related emission (industrial manufacturing, chemical feedstock, and solvent utilization)
388 together accounted for 50.0% of the total VOCs mixing ratios. The vehicle-related emission sources
389 (vehicle exhaust and gasoline evaporation), accounted for 31.7% of the total VOCs mixing ratios. It
390 indicated that traffic and industry sources were the major VOCs sources before the control period.
391 Compared with BG20, the contribution of solvent utilization was reduced to the largest extent, with a
392 magnitude of 1.43 ppbv, followed by industrial manufacturing (0.69 ppbv), and vehicle exhaust (0.38
393 ppbv), during the first emission control period (DG20 I). According to the control strategy during G20,
394 the control measures of source emission were mainly on the industry and power plant in DG20 I, and
395 thus it was responsible for the large reduction of industry-related emission including solvent utilization
396 (76.0%), industrial manufacturing (44.0%), and vehicle exhaust (21.0%). With the acceleration of
397 emission control (DG20 II), the contribution of vehicle-related emission was reduced as expected in
398 vehicle exhaust (66.1%) and gasoline evaporation (61.8%) relative to DG20 I, while significant increase
399 was also found in fuel combustion with the increment of 0.7 ppbv (152.6%). After G20, the
400 contributions of vehicle-related emission and industry-related emission both showed bounces due to
401 lifting a ban on industry, power plant, and transport in and around Zhejiang Province. It should be
402 mentioned that biogenic emission also played an indispensable importance in contributing to the VOCs
403 mixing ratios, from 0.81 ppbv to 1.29 ppbv. About 20.9% of the total VOCs mixing ratios could be
404 ascribed to the biogenic emission, acting as the second major source, during the G20 II period. It
405 indicated that biogenic VOCs might make more contribution to the VOCs mixing ratios especially when
406 anthropogenic VOCs were substantially reduced following the process of control measures.

407 Moreover, we quantified their respective ozone formation potential (OFP) before, during, and after G20
408 by using the latest maximum incremental reactivity (MIR) and the appointed concentration profiles
409 above (See Fig. 6). Overall, the total OFP in DG20 was significantly reduced by the implement of
410 stringent control measures compared with BG20 and AG20. Specifically, the OFPs of solvent utilization,
411 industrial manufacturing, and vehicle exhaust both showed significant decreases (17.3%-77.2%)



412 compared with BG20, while fuel combustion significantly increased by 52.2% with the OFP of 6.9 ppbv,
413 accounting for 25.6% of the total during G20. Thus, it is clear that the high OFP of fuel combustion
414 contributed by ethylene was also responsible for the enhanced concentration of O₃ during G20. Such
415 high OFP from fuel combustion was also elucidated in APEC in Beijing (Li et al., 2015). To classify the
416 specific fuel type, we first examined the fire spots derived from the Fire Inventory NCAR Version-1.5
417 (FINNV1.5) in eastern China before, during, and after the period of 2016 G20 (See Fig. S5 in SI). Straw
418 combustion was excluded according to the decrease in the number of fire spots in the same time period
419 from BG20 to AG20. As mentioned above, industrial process with coal combustion was strictly limited
420 throughout the whole G20 period. To ensure the clean energy used in 2016 G20, local government
421 accelerated the supply of liquid natural gas during the 13th Five-Year Plan period in Hangzhou. In 2016,
422 the consumption amounts of natural gas and liquid petroleum gas both increased up to 4.55×10⁹ kg
423 (54.4%) and 5.09×10⁸ kg (13.4%) compared with those in 2015, respectively (ZPSY, 2016, 2017). Thus,
424 liquid natural gas and petroleum gas were identified as the major fuel used in the residential usage
425 during G20. After G20, all anthropogenic sources both showed significant increments of OFP, among
426 which the fastest growth of source was vehicle exhaust (17.6 ppbv, 638.4%), followed by fuel
427 combustion (9.4 ppbv, 35.1%), industrial manufacturing (7.7 ppbv, 89.2%), and solvent utilization (7.4
428 ppbv, 258.1%), respectively.

429 **4 Conclusions**

430 In this study, ground-based concentrations of atmospheric trace gases and particulate matter, together
431 with meteorological parameters, were measured at a NRCS site in urban Hangzhou before, during, and
432 after G20. We found significant decreases in atmospheric VOCs, PM_{2.5}, NO_x, and SO₂ in DG20 relative
433 to BG20 and AG20, respectively, under the unfavorable meteorological conditions (e.g., stable weather
434 pattern and regional transport). This evidence well indicated that the powerful control measures have
435 taken effect in their emissions in Hangzhou. On the contrary, observed DMA8 O₃ increased from BG20
436 to DG20 I, which was attributed to the regional transport from the northern provinces and the enhanced
437 solar radiation intensity, and then decreased from DG20 II to AG20. The decreases in the peak
438 concentration of daily O₃ and the OFP estimated from various VOCs sources both suggested the
439 effectiveness of stringent control measures on reducing atmospheric O₃ concentrations. Unlike O₃, PAN
440 exhibited gradual decrease from BG20 to DG20. With the OBM model, we found acetaldehyde and
441 methyl glyoxal (MGLY) to be the most important second-generation precursors of PAN, accounting for
442 37.3-51.6% and 22.8%-29.5% of the total production rates including the reactions of OVOCs,
443 propagation of other radicals, and other minor sources. Furthermore, we confirmed that the production
444 of PAN was sensitive to anthropogenic and biogenic VOCs (isoprene) throughout the whole period,
445 specifically aromatics in BG20 and DG20 I but alkenes in AG20. Similarly, the sensitivity of ozone
446 formation was also under VOC-limited regime throughout G20 period. These findings suggest that



447 reducing emissions of alkanes, alkenes, and aromatics would mitigate photochemical smog including
448 PAN and O₃ formation. Furthermore, traffic (vehicle exhaust and gasoline evaporation) and industrial
449 sources (solvent utilization, industrial manufacturing, and chemical feedstock) were found to be the
450 major VOCs sources before G20, accounting for ca. 50.0% and 31.7% of the total, respectively, with the
451 ozone formation potential (OFP) of 14.4 ppbv and 16.1 ppbv. Large decreases were found in the sources
452 and OFPs of solvent utilization (74.1% and 17.3%), followed by vehicle exhaust (57.4% and 77.2%)
453 and industrial manufacturing (56.0% and 40.3%) response to the stringent control measures during G20,
454 but significantly increased by 4.2 and 2.6, 0.7 and 6.4, and 1.7 and 0.9 times after G20 due to lifting a
455 ban on industry, power plant, and transport in and around Zhejiang Province. We also appeal to pay
456 attention on controlling fuel combustion and biogenic emission especially when anthropogenic VOCs
457 were substantially reduced following the process of control measures. The experience of G20 suggests
458 that stringent emission controls do effectively address primary pollution, but a coordinated program
459 related with controlling fuel combustion and biogenic emissions is required to mitigate secondary
460 pollution.

461 **Author contributions.** GZ and HX designed research; HW, BQ, RD, and XM performed research, GZ,
462 LX, JH, WX, CL, LL, ZL, KG, YY, and WJ analyzed data; and GZ, HX, LX wrote the paper.

463 Data

464

465 **Data availability.** The data in the figures in both the main text and the Supplement are available upon
466 request to the corresponding author (Gen Zhang, zhanggen@cma.gov.cn).

467

468 **Competing interests.** The authors declare that they have no conflict of interest.

469

470 **Acknowledgements.** This study is financially supported by National Key Research and Development
471 Program of China (2016YFC0202300), National Natural Science Foundation of China (41775127 and
472 41505108), State Environmental Protection Key Laboratory of the Cause and Prevention of Urban Air
473 Pollution Complex (Y201701), and Zhejiang Provincial National Science Foundation (LY19D050002).
474 The authors are especially grateful to Dr. Xiaobin Xu for the help in discussions.



475 **References**

- 476 Cai, C., Geng, F., Tie, X., Yu, Q., and An, J.: Characteristics and source apportionment of VOCs
477 measured in Shanghai, China, *Atmos. Environ.*, 44, 5005-5014, 2010.
- 478 Chameides, W. L., Xingsheng, L., Xiaoyan, T., Xiuji, Z., Luo, C., Kiang, C. S., St. John, J., Saylor, R.
479 D., Liu, S. C., Lam, K. S., Wang, T., and Giorgi, F.: Is ozone pollution affecting crop yields in China?,
480 *Geophys.Res. Lett.*, 26, 867-870, 1999.
- 481 Cheng, Y. F., Zheng, G. J., Wei, C., Mu, Q., Zheng, B., Wang, Z. B., Gao, M., Zhang, Q., He, K. B.,
482 Carmichael, G., Poschl, U., and Su, H.: Reactive nitrogen chemistry in aerosol water as a source of
483 sulfate during haze events in China, *Sci. Adv.*, 2, 2016.
- 484 de Foy, B., Lu, Z. F., and Streets, D. G.: Satellite NO₂ retrievals suggest China has exceeded its NO_x
485 reduction goals from the twelfth Five-Year Plan, *Sci Rep-Uk*, 6,35912, 2016.
- 486 Ding, A. J., Fu, C. B., Yang, X. Q., Sun, J. N., Zheng, L. F., Xie, Y. N., Herrmann, E., Nie, W., Petäjä, T.,
487 Kerminen, V. M., and Kulmala, M.: Ozone and fine particulate in the western Yangtze River Delta: an
488 overview of 1 yr data at the SORPES station, *Atmos. Chem. Phys.*, 13, 5813-5830, 2013.
- 489 Feng, C., Gao, X., Tang, Y., and Zhang, Y.: Comparative life cycle environmental assessment of flue gas
490 desulphurization technologies in China, *J. Clean. Prod.*, 68, 81-92, 2014.
- 491 Gao, Y., Liu, X., Zhao, C., and Zhang, M.: Emission controls versus meteorological conditions in
492 determining aerosol concentrations in Beijing during the 2008 Olympic Games, *Atmos. Chem. Phys.*, 11,
493 12437-12451, 2011.
- 494 Geng, F. H., Zhao, C. S., Tang, X., Lu, G. L., and Tie, X. X.: Analysis of ozone and VOCs measured in
495 Shanghai: A case study, *Atmos. Environ.*, 41, 989-1001, 2007.
- 496 Guenther, A., Hewitt, C. N., Erickson, D., Fall, R., Geron, C., Graedel, T., Harley, P., Klinger, L.,
497 Manuel, L., McKay, W. A., Pierce, T., Scholes, B., Steinbrecher, R., Tallamraju, R., Taylor, J., and
498 Zimmerman, P.: A global model of natural volatile organic compound emissions, *J. Geophys.*
499 *Res-Atmos.*, 100, 8873-8892, 1995.
- 500 Hopke, P. K.: Recent developments in receptor modeling, *J. Chemometr.*, 17, 255-265, 2003.
- 501 Huang, R. J., Zhang, Y. L., Bozzetti, C., Ho, K. F., Cao, J. J., Han, Y. M., Daellenbach, K. R., Slowik, J.
502 G., Platt, S. M., Canonaco, F., Zotter, P., Wolf, R., Pieber, S. M., Bruns, E. A., Crippa, M., Ciarelli, G.,
503 Piazzalunga, A., Schwikowski, M., Abbaszade, G., Schnelle-Kreis, J., Zimmermann, R., An, Z. S.,
504 Szidat, S., Baltensperger, U., El Haddad, I., and Prevot, A. S. H.: High secondary aerosol contribution to
505 particulate pollution during haze events in China, *Nature*, 514, 218-222, 2014.
- 506 Jenkin, M. E., Saunders, S. M., Wagner, V., and Pilling, M. J.: Protocol for the development of the
507 Master Chemical Mechanism, MCM v3 (Part B): tropospheric degradation of aromatic volatile organic
508 compounds, *Atmos. Chem. Phys.*, 3, 181-193, 2003.
- 509 Kondo, Y., Morino, Y., Fukuda, M., Kanaya, Y., Miyazaki, Y., Takegawa, N., Tanimoto, H., McKenzie,
510 R., Johnston, P., Blake, D. R., Murayama, T., and Koike, M.: Formation and transport of oxidized



511 reactive nitrogen, ozone, and secondary organic aerosol in Tokyo, *J. Geophys. Res.-Atmos.*, 113, 2008.

512 Koukoulis, M. E., Balis, D. S., van der A, R. J., Theys, N., Hedelt, P., Richter, A., Krotkov, N., Li, C.,
513 and Taylor, M.: Anthropogenic sulphur dioxide load over China as observed from different satellite
514 sensors, *Atmos. Environ.*, 145, 45-59, 2016.

515 LaFranchi, B. W., Wolfe, G. M., Thornton, J. A., Harrold, S. A., Browne, E. C., Min, K. E., Wooldridge,
516 P. J., Gilman, J. B., Kuster, W. C., Goldan, P. D., de Gouw, J. A., McKay, M., Goldstein, A. H., Ren, X.,
517 Mao, J., and Cohen, R. C.: Closing the peroxy acetyl nitrate budget: observations of acyl peroxy nitrates
518 (PAN, PPN, and MPAN) during BEARPEX 2007, *Atmos. Chem. Phys.*, 9, 7623-7641, 2009.

519 Lelieveld, J., Evans, J. S., Fnais, M., Giannadaki, D., and Pozzer, A.: The contribution of outdoor air
520 pollution sources to premature mortality on a global scale, *Nature*, 525, 367-371, 2015.

521 Li, J., Xie, S. D., Zeng, L. M., Li, L. Y., Li, Y. Q., and Wu, R. R.: Characterization of ambient volatile
522 organic compounds and their sources in Beijing, before, during, and after Asia-Pacific Economic
523 Cooperation China 2014, *Atmos. Chem. Phys.*, 15, 7945-7959, 2015.

524 Li, L., An, J. Y., Shi, Y. Y., Zhou, M., Yan, R. S., Huang, C., Wang, H. L., Lou, S. R., Wang, Q., Lu, Q.,
525 and Wu, J.: Source apportionment of surface ozone in the Yangtze River Delta, China in the summer of
526 2013, *Atmos. Environ.*, 144, 194-207, 2016.

527 Li, K., Li, J., Wang, W., Tong, S., Liggio, J., and Ge, M.: Evaluating the effectiveness of joint emission
528 control policies on the reduction of ambient VOCs: Implications from observation during the 2014
529 APEC summit in suburban Beijing, *Atmos. Environ.*, 164, 117-127, 2017.

530 Li, Z., Xue, L., Yang, X., Zha, Q., Tham, Y. J., Yan, C., Louie, P. K. K., Luk, C. W. Y., Wang, T., and
531 Wang, W.: Oxidizing capacity of the rural atmosphere in Hong Kong, Southern China, *Sci. Total
532 Environ.*, 612, 1114-1122, 2018.

533 Liu, Y., Shao, M., Fu, L., Lu, S., Zeng, L., and Tang, D.: Source profiles of volatile organic compounds
534 (VOCs) measured in China: Part I, *Atmos. Environ.*, 42, 6247-6260, 2008.

535 Liu, Z., Wang, Y. H., Gu, D. S., Zhao, C., Huey, L. G., Stickel, R., Liao, J., Shao, M., Zhu, T., Zeng, L.
536 M., Liu, S. C., Chang, C. C., Amoroso, A., and Costabile, F.: Evidence of reactive aromatics as a major
537 source of peroxy acetyl nitrate over China, *Environ. Sci. Technol.*, 44, 7017-7022, 2010.

538 McCarthy, M. C., Aklilu, Y.-A., Brown, S. G., and Lyder, D. A.: Source apportionment of volatile
539 organic compounds measured in Edmonton, Alberta, *Atmos. Environ.*, 81, 504-516, 2013.

540 McFadyen, G. G., and Cape, J. N.: Peroxyacetyl nitrate in eastern Scotland, *Sci Total Environ*, 337,
541 213-222, 2005.

542 Miao, Y. C., and Liu, S. H.: Linkages between aerosol pollution and planetary boundary layer structure
543 in China, *Sci. Total Environ.*, 650, 288-296, 2019.

544 Miao, Y. C., Liu, S. H., Guo, J. P., Huang, S. X., Yan, Y., and Lou, M. Y.: Unraveling the relationships
545 between boundary layer height and PM_{2.5} pollution in China based on four-year radiosonde
546 measurements, *Environ. Pollut.*, 243, 1186-1195, 2018.



- 547 Mo, Z., Shao, M., Lu, S., Qu, H., Zhou, M., Sun, J., and Gou, B.: Process-specific emission
548 characteristics of volatile organic compounds (VOCs) from petrochemical facilities in the Yangtze River
549 Delta, China, *Sci. Total Environ.*, 533, 422-431, 2015.
- 550 Pentti, P., and Unto, T.: Positive matrix factorization: a non-negative factor model with optimal
551 utilization of error estimates of data values, *Environmetrics*, 5, 111-126, 1994.
- 552 Roberts, J. M., Stroud, C. A., Jobson, B. T., Trainer, M., Hereid, D., Williams, E., Fehsenfeld, F., Brune,
553 W., Martinez, M., and Harder, H.: Application of a sequential reaction model to PANs and aldehyde
554 measurements in two urban areas, *Geophys. Res. Lett.*, 28, 4583-4586, 2001.
- 555 Saunders, S. M., Jenkin, M. E., Derwent, R. G., and Pilling, M. J.: Protocol for the development of the
556 Master Chemical Mechanism, MCM v3 (Part A): tropospheric degradation of non-aromatic volatile
557 organic compounds, *Atmos. Chem. Phys.*, 3, 161-180, 2003.
- 558 Shao, M., Lu, S. H., Liu, Y., Xie, X., Chang, C. C., Huang, S., and Chen, Z. M.: Volatile organic
559 compounds measured in summer in Beijing and their role in ground-level ozone formation, *J. Geophys.*
560 *Res.-Atmos.*, 114, 2009.
- 561 Verstraeten, W. W., Neu, J. L., Williams, J. E., Bowman, K. W., Worden, J. R., and Boersma, K. F.:
562 Rapid increases in tropospheric ozone production and export from China, *Nat. Geosci.*, 8, 690-695,
563 2015.
- 564 Wang, Q., Geng, C., Lu, S., Chen, W., and Shao, M.: Emission factors of gaseous carbonaceous species
565 from residential combustion of coal and crop residue briquettes, *Front. Environ. Sci. Eng.*, 7, 66-76,
566 2013.
- 567 Wang, T., Xue, L. K., Brimblecombe, P., Lam, Y. F., Li, L., and Zhang, L.: Ozone pollution in China: A
568 review of concentrations, meteorological influences, chemical precursors, and effects, *Sci. Total.*
569 *Environ.*, 575, 1582-1596, 2017.
- 570 Wang, Y. G., Ying, Q., Hu, J. L., and Zhang, H. L.: Spatial and temporal variations of six criteria air
571 pollutants in 31 provincial capital cities in China during 2013-2014, *Environ. Int.*, 73, 413-422, 2014.
- 572 Wang, Y. Q., Zhang, X. Y., Arimoto, R., Cao, J. J., and Shen, Z. X.: The transport pathways and sources
573 of PM₁₀ pollution in Beijing during spring 2001, 2002 and 2003, *Geophys. Res. Lett.*, 31, 2004.
- 574 Watson, J. G., Chow, J. C., and Fujita, E. M.: Review of volatile organic compound source
575 apportionment by chemical mass balance, *Atmos. Environ.*, 35, 1567-1584, 2001.
- 576 Williams, J., Roberts, J. M., Bertman, S. B., Stroud, C. A., Fehsenfeld, F. C., Baumann, K., Buhr, M. P.,
577 Knapp, K., Murphy, P. C., Nowick, M., and Williams, E. J.: A method for the airborne measurement of
578 PAN, PPN, and MPAN, *J. Geophys. Res.-Atmos.*, 105, 28943-28960, 2000.
- 579 Xu, Z., Liu, J. F., Zhang, Y. J., Liang, P., and Mu, Y. J.: Ambient levels of atmospheric carbonyls in
580 Beijing during the 2008 Olympic Games, *J. Environ. Sci.*, 22, 1348-1356, 2010.
- 581 Xue, L., Gu, R., Wang, T., Wang, X., Saunders, S., Blake, D., Louie, P. K. K., Luk, C. W. Y., Simpson, I.,
582 Xu, Z., Wang, Z., Gao, Y., Lee, S., Mellouki, A., and Wang, W.: Oxidative capacity and radical



583 chemistry in the polluted atmosphere of Hong Kong and Pearl River Delta region: analysis of a severe
584 photochemical smog episode, *Atmos. Chem. Phys.*, 16, 9891-9903, 2016.

585 Xue, L. K., Wang, T., Louie, P. K. K., Luk, C. W. Y., Blake, D. R., and Xu, Z.: Increasing external
586 effects negate local efforts to control ozone air pollution: a case study of Hong Kong and implications
587 for other Chinese cities, *Environ. Sci. Technol.*, 48, 10769-10775, 2014a.

588 Xue, L. K., Wang, T., Gao, J., Ding, A. J., Zhou, X. H., Blake, D. R., Wang, X. F., Saunders, S. M., Fan,
589 S. J., Zuo, H. C., Zhang, Q. Z., and Wang, W. X.: Ground-level ozone in four Chinese cities: precursors,
590 regional transport and heterogeneous processes, *Atmos. Chem. Phys.*, 14, 13175-13188, 2014b.

591 Xue, L. K., Wang, T., Wang, X. F., Blake, D. R., Gao, J., Nie, W., Gao, R., Gao, X. M., Xu, Z., Ding, A.
592 J., Huang, Y., Lee, S. C., Chen, Y. Z., Wang, S. L., Chai, F. H., Zhang, Q. Z., and Wang, W. X.: On the
593 use of an explicit chemical mechanism to dissect peroxy acetyl nitrate formation, *Environ. Pollut.*, 195,
594 39-47, 2014c.

595 Yang, G. H., Wang, Y., Zeng, Y. X., Gao, G. F., Liang, X. F., Zhou, M. G., Wan, X., Yu, S. C., Jiang, Y.
596 H., Naghavi, M., Vos, T., Wang, H. D., Lopez, A. D., and Murray, C. J. L.: Rapid health transition in
597 China, 1990-2010: findings from the Global Burden of Disease Study 2010, *Lancet*, 381, 1987-2015,
598 2013.

599 Zhang, G., Mu, Y. J., Liu, J. F., and Mellouki, A.: Direct and simultaneous determination of trace-level
600 carbon tetrachloride, peroxyacetyl nitrate, and peroxypropionyl nitrate using gas
601 chromatography-electron capture detection, *J. Chromatogr. A*, 1266, 110-115, 2012a.

602 Zhang, G., Mu, Y. J., Liu, J. F., Zhang, C. L., Zhang, Y. Y., Zhang, Y. J., and Zhang, H. X.: Seasonal and
603 diurnal variations of atmospheric peroxyacetyl nitrate, peroxypropionyl nitrate, and carbon tetrachloride
604 in Beijing, *J. Environ. Sci.*, 26, 65-74, 2014.

605 Zhang, G., Mu, Y. J., Zhou, L. X., Zhang, C. L., Zhang, Y. Y., Liu, J. F., Fang, S. X., and Yao, B.:
606 Summertime distributions of peroxyacetyl nitrate (PAN) and peroxypropionyl nitrate (PPN) in Beijing:
607 Understanding the sources and major sink of PAN, *Atmos. Environ.*, 103, 289-296, 2015.

608 Zhang, G., Xu, H. H., Qi, B., Du, R. G., Gui, K., Wang, H. L., Jiang, W. T., Liang, L. L., and Xu, W. Y.:
609 Characterization of atmospheric trace gases and particulate matter in Hangzhou, China, *Atmos. Chem.*
610 *Phys.*, 18, 1705-1728, 2018.

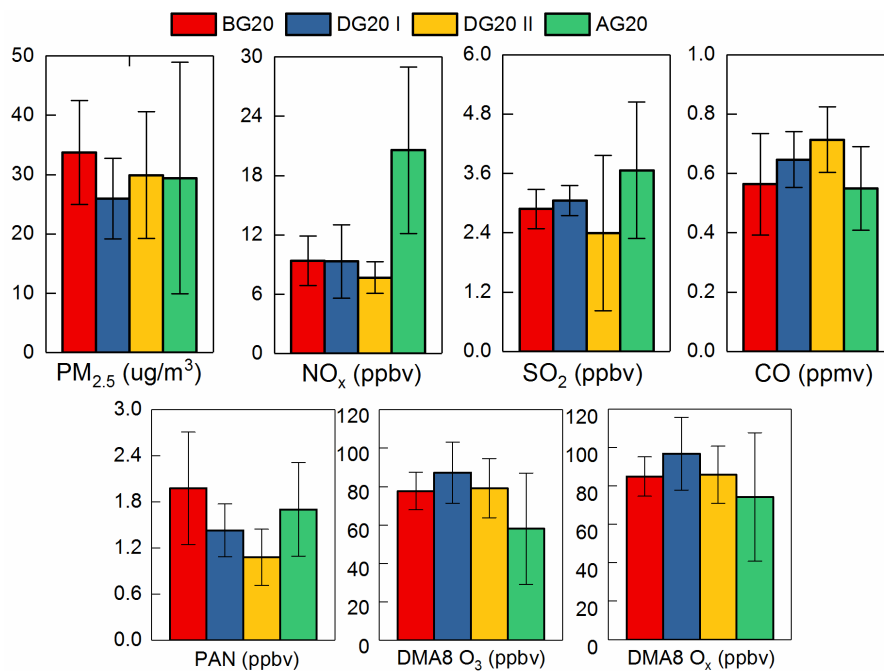
611 Zhang, H., Wang, S., Hao, J., Wang, X., Wang, S., Chai, F., and Li, M.: Air pollution and control action
612 in Beijing, *J. Clean. Prod.*, 112, 1519-1527, 2016.

613 Zhang, R., Jing, J., Tao, J., Hsu, S. C., Wang, G., Cao, J., Lee, C. S. L., Zhu, L., Chen, Z., Zhao, Y., and
614 Shen, Z.: Chemical characterization and source apportionment of PM_{2.5} in Beijing: seasonal
615 perspective, *Atmos. Chem. Phys.*, 13, 7053-7074, 2013.

616 Zhang, Y. J., Mu, Y. J., Liang, P., Xu, Z., Liu, J. F., Zhang, H. X., Wang, X. K., Gao, J., Wang, S. L.,
617 Chai, F. H., and Mellouki, A.: Atmospheric BTEX and carbonyls during summer seasons of 2008-2010
618 in Beijing, *Atmos. Environ.*, 59, 186-191, 2012b.



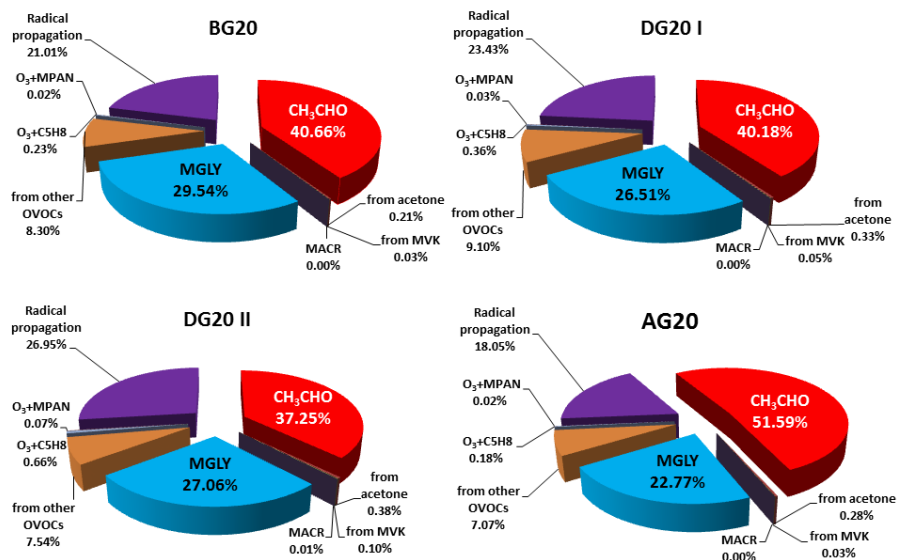
- 619 Zhejiang Province Statistics Yearbook, 2016.
620 Zhejiang Province Statistics Yearbook, 2017.
621



622

623 Figure 1. The comparisons of daytime PM_{2.5}, NO_x, SO₂, CO, PAN, DMA8 O₃, and DMA8 O_x. before,
624 during, and after G20, denoted as BG20, DG20, and AG20, respectively. The error bars represent the
625 standard deviations.

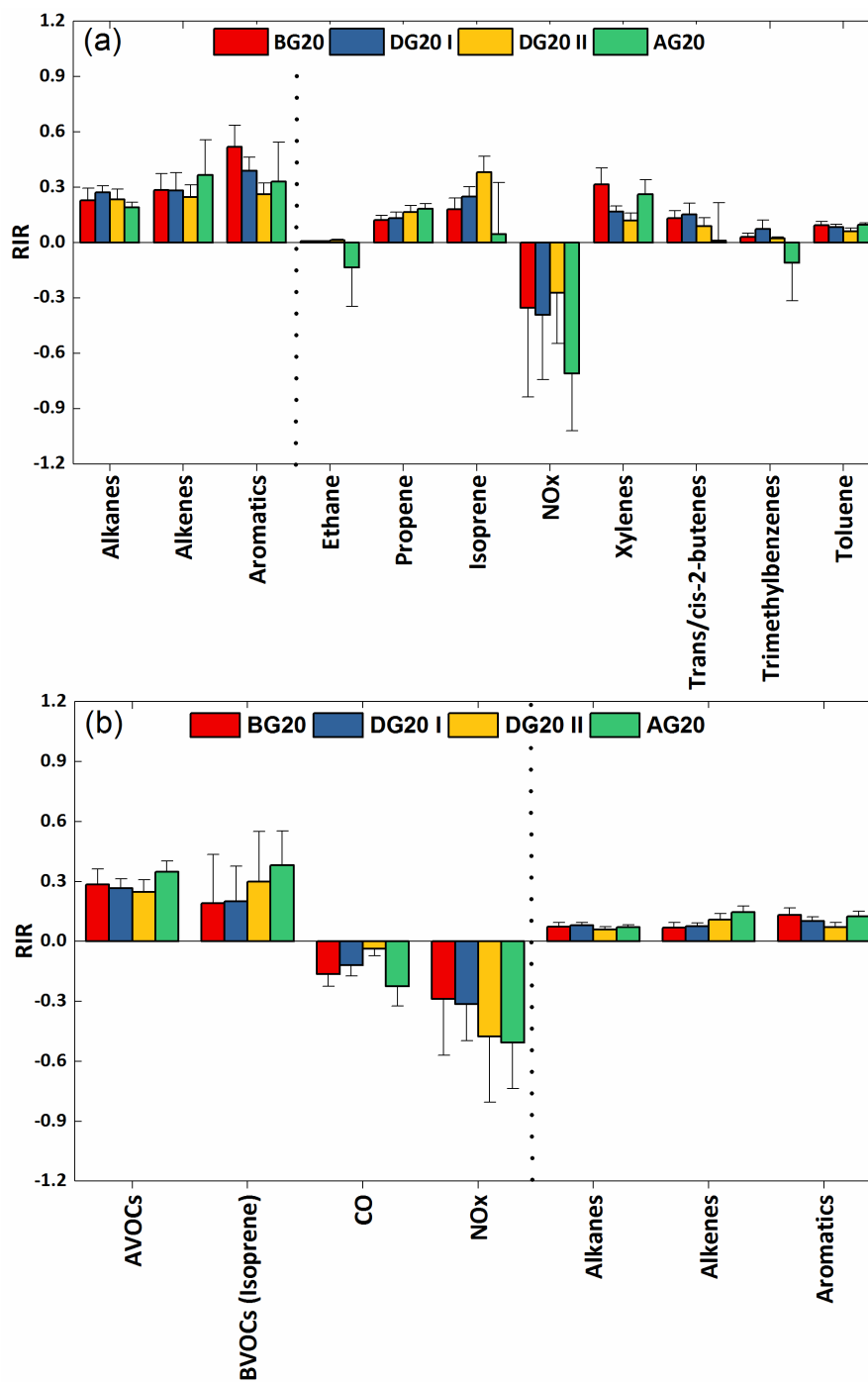
626



627

628 Figure 2. Contributions of individual pathways to PA radical formation during the episodes of BG20,
629 DG20 I, DG20 II, and AG20, respectively.

630



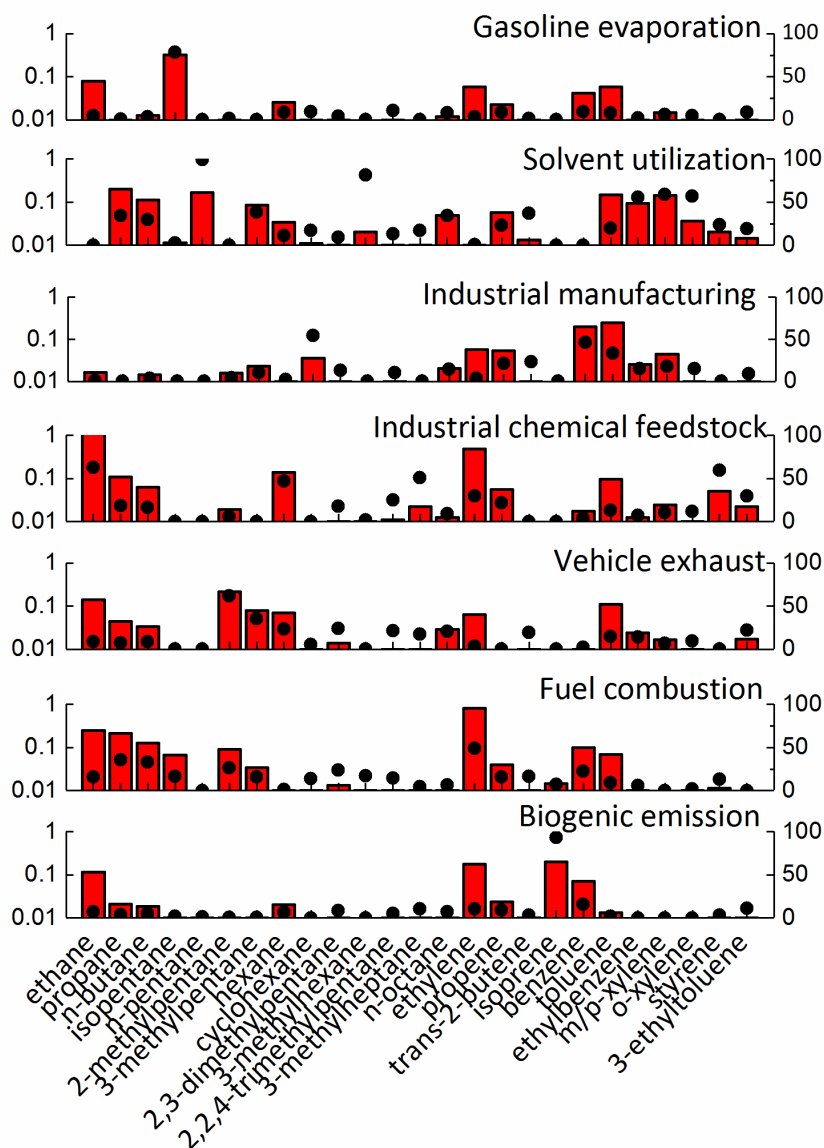
631

632 Figure 3. Sensitivity of PAN (a) and O₃ (b) production rate to major precursor groups and individual

633

species (09:00-17:00). Error bars are standard deviations.

634



635

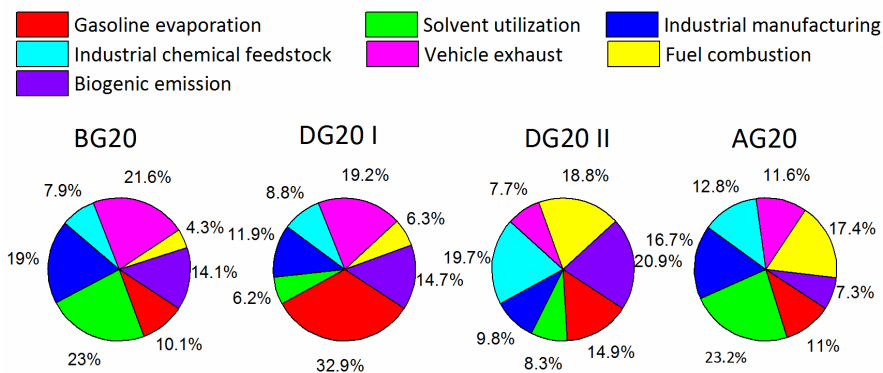
636 Figure 4. Seven source profiles and their respective contribution resolved from PMF model. The bars

637 are the profiles (ppbv, left axis), and the dots are the percentage contribution (% ,right axis) from

638

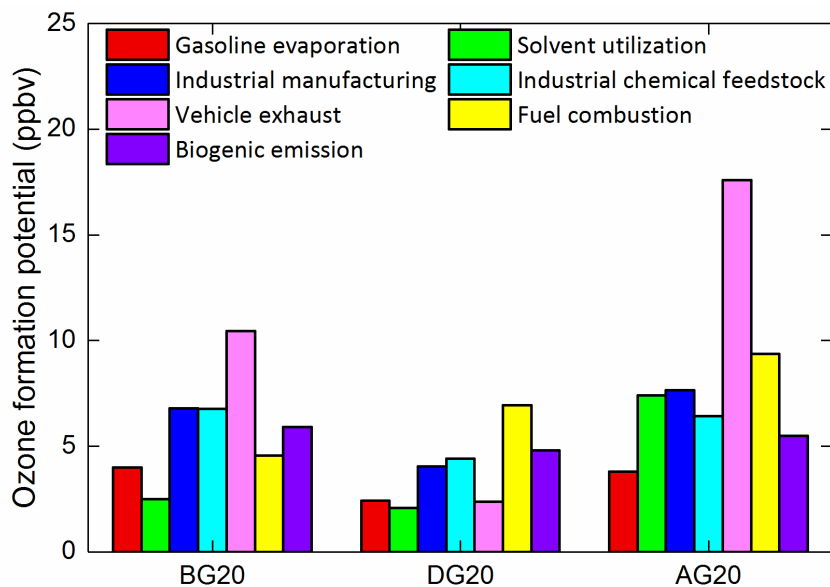
individual factor.

639



640
641
642

Figure 5. Variation of the sources (percentage) during the four periods



643

644 Figure 6. Ozone formation potential (ppbv) of each source before, during, and after the control period

645

during 2016 G20 in China